catalysts

MDPI

Article

Shape-Dependent Catalytic Activity of Gold and Bimetallic Nanoparticles in the Reduction of Methylene Blue by Sodium Borohydride

Heike Lisa Kerstin Stephanie Stolle [1], Jonas Jakobus Kluitmann [2], Andrea Csáki [1], Johann Michael Köhler [2] and Wolfgang Fritzsche [1,*]

[1] Department of Nanobiophotonics, Leibniz Institute of Photonic Technology (IPHT), Albert-Einstein-Straße 9, 07745 Jena, Germany; lisa.stolle@leibniz-ipht.de (H.L.K.S.S.); andrea.csaki@leibniz-ipht.de (A.C.)
[2] Department of Physical Chemistry and Microreaction Technology, Institute for Micro and Nanotechnologies/Institute for Chemistry and Biotechnology, Technische Universität Ilmenau, P.O. Box 10 05 65, 98694 Ilmenau, Germany; jonas.kluitmann@tu-ilmenau.de (J.J.K.); michael.koehler@tu-ilmenau.de (J.M.K.)
* Correspondence: wolfgang.fritzsche@leibniz-ipht.de

Abstract: In this study the catalytic activity of different gold and bimetallic nanoparticle solutions towards the reduction of methylene blue by sodium borohydride as a model reaction is investigated. By utilizing differently shaped gold nanoparticles, i.e., spheres, cubes, prisms and rods as well as bimetallic gold–palladium and gold–platinum core-shell nanorods, we evaluate the effect of the catalyst surface area as available gold surface area, the shape of the nanoparticles and the impact of added secondary metals in case of bimetallic nanorods. We track the reaction by UV/Vis measurements in the range of 190–850 nm every 60 s. It is assumed that the gold nanoparticles do not only act as a unit transferring electrons from sodium borohydride towards methylene blue but can promote the electron transfer upon plasmonic excitation. By testing different particle shapes, we could indeed demonstrate an effect of the particle shape by excluding the impact of surface area and/or surface ligands. All nanoparticle solutions showed a higher methylene blue turnover than their reference, whereby gold nanoprisms exhibited 100% turnover as no further methylene blue absorption peak was detected. The reaction rate constant k was also determined and revealed overall quicker reactions when gold or bimetallic nanoparticles were added as a catalyst, and again these were highest for nanoprisms. Furthermore, when comparing gold and bimetallic nanorods, it could be shown that through the addition of the catalytically active second metal platinum or palladium, the dye turnover was accelerated and degradation rate constants were higher compared to those of pure gold nanorods. The results explore the catalytic activity of nanoparticles, and assist in exploring further catalytic applications.

Keywords: metal nanoparticles; shape-anisotropic nanoparticles; bimetallic nanoparticles; quasi-homogeneous catalysis; methylene blue reduction; UV/Vis spectroscopy

Citation: Stolle, H.L.K.S.; Kluitmann, J.J.; Csáki, A.; Köhler, J.M.; Fritzsche, W. Shape-Dependent Catalytic Activity of Gold and Bimetallic Nanoparticles in the Reduction of Methylene Blue by Sodium Borohydride. *Catalysts* **2021**, *11*, 1442. https://doi.org/10.3390/catal11121442

Academic Editors: Biljana F. Abramovic and Tamara B. Ivetić

Received: 15 October 2021
Accepted: 23 November 2021
Published: 26 November 2021

1. Introduction

Plasmonic metal nanoparticles show the interesting effect of so-called localized surface plasmon resonance (LSPR) [1]: free electrons in the metal nanoparticle start to oscillate in a collective through the impact of light of wavelengths resonant to the frequency of the oscillation of the electrons against the restoring forces of the metal cores [2]. This movement is called "plasmon" [3–5], whereby the collective of electrons is moving over the entire volume of the metal nanoparticle and causes an oscillating dipole [3,4]. The LSPR excitation results in different relaxation processes, ranging from enhancement of the electrical field around the nanoparticle [6,7] to the generation of electron-hole pairs through raising electrons to a higher state [8,9]. These charge carriers can then be passed on to surrounding

molecules and induce reduction, respectively, and oxidation processes [10,11]. Plasmon heating through interactions from the moving electrons with the metal lattice is also possible [12], causing thermally induced changes of the particle itself or its environment [6]. Lastly, the irradiated photon can simply be scattered, which is especially the case for larger particles [13].

The synthesis of these particles is possible through different approaches either as monometallic or bimetallic nanoparticles. The typically utilized bottom-up technique including metal salts and different reducing agents involves classical [14–20] or microfluidic [21–25] wet-chemical synthesis approaches, or preparation through ball milling [26–29]. Furthermore, gold nanoparticles in particular can be synthesized in different shapes, such as spheres [14,16–18], cubes [30], rods [31,32], prisms [33,34] or stars [35]. Hereby, the principle of *seeded-growth* plays an important role. In this technique, strong and weak reducing agents are utilized in different synthesis steps [36]. Small seed particles are synthesized by utilizing a stronger reducing agent, whereas the final particle size is adjusted by the volume of added seeds and weaker reducing agents in the following step(s) [30,32,34]. This method leads to a narrower particle size distribution than a simple one-step process [37]. *Seeded-growth* is especially important when it comes to the synthesis of shape-anisotropic nanoparticles. In order to obtain shape-anisotropic particles, the application of surfactants is essential [22,32,38]. Such surfactants as cetyltrimethylammonium bromide (CTAB) or -chloride (CTAC) need to be added already in seed synthesis and lead in the following steps to the formation of desired shapes [23,30,32,39]. Thereby, the CTA^+ ion sterically blocks favorably the {110}-facets, followed by {100}- and {111}-facets of gold crystals, which leads to a crystal growth of only the free facets [38]. The resulting shape is furthermore also strongly dependent on the counter ions added. For example, gold nanorods only result when bromide is used [38,40], whereas cubes require low bromide concentration, which is why CTAC is used [22,23,30], and nanoprism synthesis necessitates iodide ions [33,34,39]. In case of bimetallic nanoparticles, *seeded-growth* is the method of choice, when the synthesis of well-defined core-shell particles [41,42] or dimers is intended [43]. Furthermore, stabilizers and surfactants are utilized in order to obtain a certain structure [19].

The LSPR-effect makes plasmonic nanoparticles interesting materials for many kinds of applications, such as bioanalytical sensing, as changes in the particle environment can be tracked by the shift of the LSPR-peak position [3,44–48]. Other analytical applications rather utilize the field-enhancing effect of the activated particles, involving surface-enhanced Raman scattering [49–52], tip-enhanced Raman scattering [53,54], metal-enhanced fluorescence measurements or surface-enhanced IR absorption [55]. Medical applications are also possible, such as in tumor treatment, mainly based on plasmon heating [56,57], drug-delivery [58] or diagnostics [3]. Furthermore, plasmonic nanoparticles represent interesting catalysts for different plasmon-mediated (photo)catalytic reactions [13,59–63]. Mechanisms for the photocatalytic reactions include plasmonic heating [59], as well as the formation of charge carriers, especially high-energetic electrons, that can catalyze a plenitude of reactions [9,62,64]. Therefore, plasmonic nanoparticles can be applied in homogeneous/heterogeneous and also electro catalysis [36,65]. This also pertains to bimetallic nanoparticles, which combine two metals and therefore exhibit other optical, electronical, thermal and catalytic qualities than monometallic nanoparticles and make them interesting materials for, e.g., applications in photocatalysis [19,66]. In this way, the combination of gold with a catalytically very active metal, e.g., palladium, leads to an interesting catalytic system, since gold can act as an antenna, effectively harvesting the light of visible wavelengths, being activated and passing on electrons to the second metal, enhancing its catalytic activity [67,68]. Similarly, the combination with the catalytically active platinum leads to an interesting catalyst material [69]. Shape-anisotropic nanoparticles are also of special interest, as their tips, edges and corners represent areas, accumulating electrons after plasmonic excitation, leading to hot spots [1,2,7]. The field enhancement of a gold nanosphere is around six times higher than the field strength of the applied photons [70]; in case of shape-anisotropic nanoparticles it can even be 500 [1] to 1000 times higher [13].

In catalysis, particles with features like the mentioned edges, tips and corners with a high number of easily accessible surface atoms proved to be catalytically very active [71,72]. Furthermore, these regions on particles seem to be beneficial for the adsorption of the substance to be catalyzed and therefore guarantee maximum contact to the catalytic active centers [73].

When it comes to catalytic applications of plasmonic nanoparticles, heterogeneous reactions are difficult to realize since they require the immobilization of particles on a catalyst carrier [9,59,60,64]. Homogeneous or quasi-homogeneous reactions can however be easily carried out, since the particles can simply remain in solution. That way, Suzuki-coupling reactions [71,74,75], oxidation reactions of different organic compounds [10,76] or H_2-generation of water could be catalyzed by (bi)metallic nanoparticles [77]. Additionally, different shape-anisotropic, CTAB-coated gold nanoparticles were tested for the reduction of 4-nitroaniline with sodium borohydride, where among the tested gold nanorods, -prisms and -spheres the latter mentioned showed the highest turnover [78]. Likewise, dyes can easily be degraded by the catalytic influence of plasmonic nanoparticles. These reactions represent a straightforward model reaction for evaluating the catalytic efficiency of different nanoparticles, as they can simply be monitored by UV/Vis measurements. In this way, methylene blue was degraded in presence of Au nanospheres and AgAu nanorings respectively. Maximum turnover was achieved after 5 h (nanorings) and 10 h (nanospheres). The mechanism of dye degradation was in this case based on plasmon-mediated formation of reactive oxygen species and subsequent methylene blue oxidation [79]. Other studies investigated the catalytic degradation of different dyes with plasmonic nanoparticles in presence of sodium borohydride. The assumed reaction mechanism involves the adsorption of the dye molecules at the catalyst surface, the hydrogen evolution and the electron transfer through oxidation of sodium borohydride prior to the transfer of electrons (and hydrogen ions) over the plasmonic nanoparticles towards the dye molecules. The electron transfer is therefore catalyzed by the nanoparticles and together with hydrogen uptake results in the dye reduction [80,81]. The catalytic mechanism can generally be described as a Langmuir–Hinshelwood mechanism, since all reactants are adsorbed on the catalyst surface and undergo a reaction there before desorbing [80]. For example, catalytic tests were carried out, in which gold nanospheres and -rods were used to catalyze the *p*-nitrophenol reduction also in presence of sodium borohydride. In this case, gold nanorods were found to be more catalytic reactive than nanospheres [72]. In studies with silver nanoparticles, the degradation of the dyes methyl orange, methylene blue and eosin Y was evaluated. Without nanoparticles, the reduction effect was only little, but increased strongly in the experiments with nanoparticles. Notably, small nanoparticles with a high surface-to-volume ratio showed quick degradation times of only six minutes [82]. Piella et al. found similar effects when utilizing gold nanospheres of different sizes for the degradation of dyes such as methylene blue, 4-nitrophenole and rhodamine B. Silver and platinum nanospheres were also tested, revealing an overall quicker and complete reduction with platinum nanoparticles, followed by gold and silver nanoparticles. In case of gold nanospheres, different surface ligands were tested and it could be found that ligands strongly bonded to the particle surface like SH-PEG (3500) or polyvinylpyrrolidone (PVP) hinder an effective reduction reaction, since the reagent could not reach the catalyst surface, whereas particles with loosely bound sodium citrate initiated an efficient and quick dye degradation [80].

In this study we investigated the catalytic performance of differently shaped gold nanoparticles and bimetallic nanorods in the model reaction of methylene blue degradation in presence of sodium borohydride. In our experiments, we sought to distinguish the catalytic efficiency of shape-isotropic and -anisotropic particles, to research the impact of the addition of a second metal and also carefully evaluated the reductive effect of surface ligands CTAC and CTAB necessary for the synthesis of shape-anisotropic nanoparticles in this model reaction easily monitored by UV/Vis-measurements.

2. Results and Discussions

2.1. Size, Shape and Optical Properties of Mono- and Bimetallic Nanoparticle Catalysts

SEM-images and absorption spectra of all utilized nanoparticle samples are displayed in Figure 1, revealing structure, size and the absorption wavelength respectively.

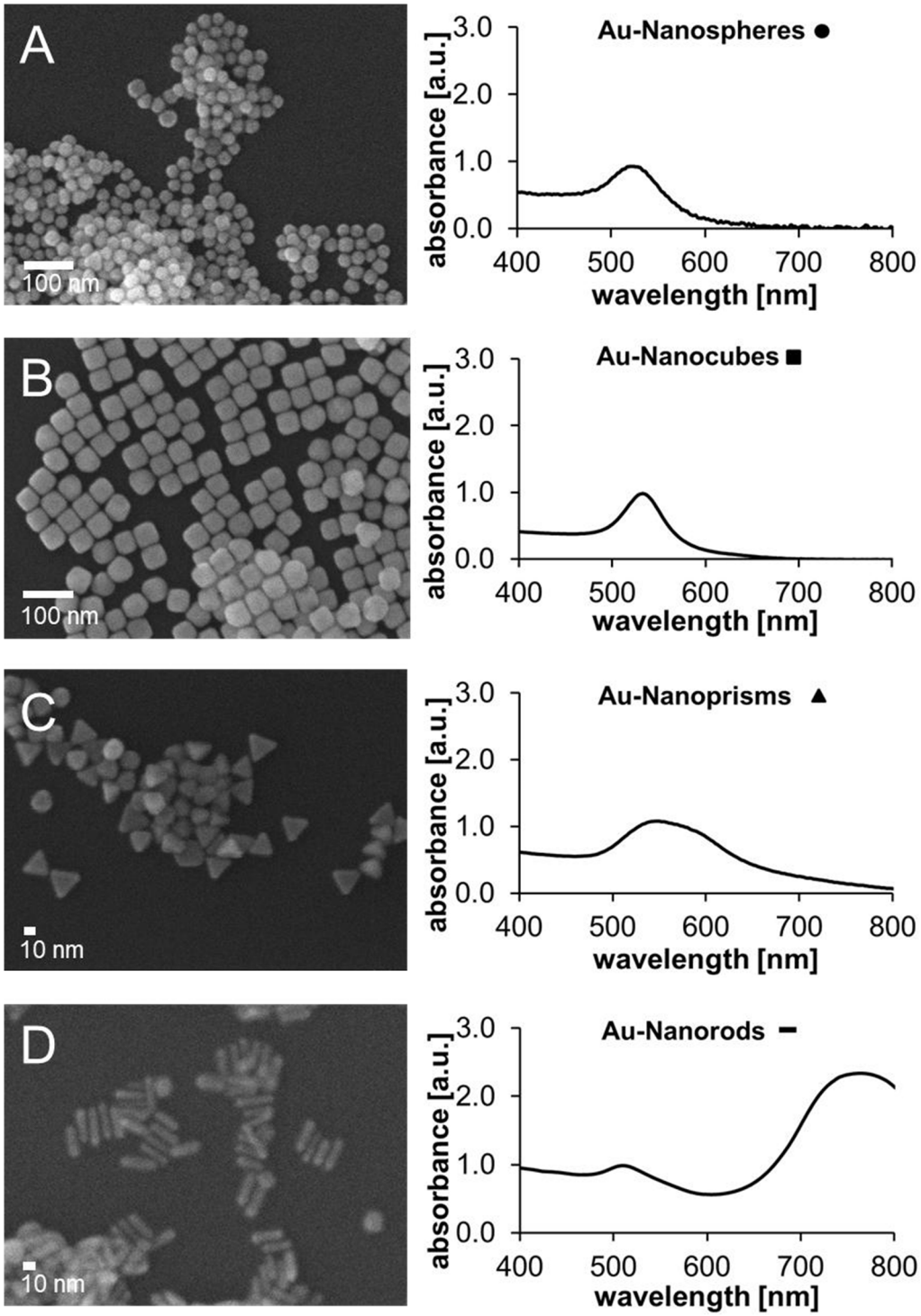

Figure 1. *Cont.*

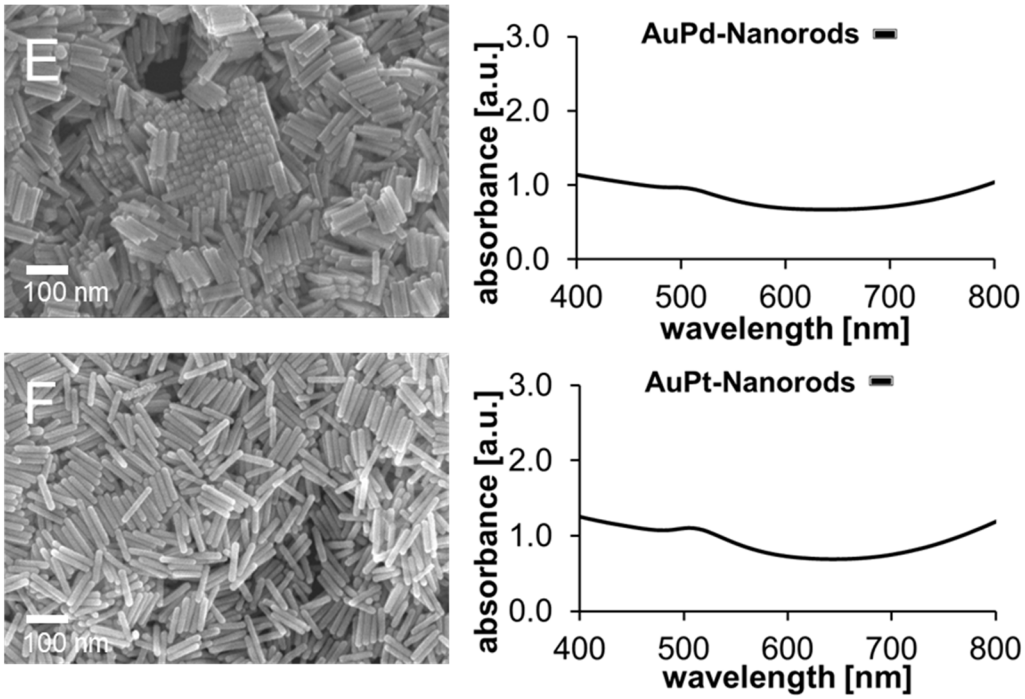

Figure 1. SEM images (**left**) of the nanoparticle samples ((**A**) = Au spheres, (**B**) = Au cubes, (**C**) = Au prisms, (**D**) = Au rods, (**E**) = AuPd rods, (**F**) = AuPt rods) and respective absorption spectra (**right**).

The citrate-stabilized gold nanospheres were relatively homogeneous with respect to size and shape, with an average diameter of 27 nm with maximum/minimum size deviation of + 10/−5.9 nm. The maximum absorption wavelength was 525 nm (Figure 1A). The gold nanocubes with CTAC shells were obtained homogeneously in size and shape and showed an absorption maximum at 533 nm and an average edge length of 41 nm (+7.4/−7.1 nm), see Figure 1B. The nanoprisms with CTAC shell showed an excitation maximum at 549 nm (Figure 1C). The edge of the prisms was on average 7.85 nm (+2.2/−1.9 nm) thick and the sides of the equilateral triangle were 20 nm (+3.9/−4.2 nm) long. With the exception of a few other particle shapes, the nanoprisms could also be obtained as a homogeneous particle sample. The synthesis of gold nanorods with CTAB was also successful with good homogeneity in terms of size and shape (see Figure 1D). Only a few deviating particle shapes were observed in the SEM image. In contrast to spheres, cubes and prisms, the nanorods exhibited two absorption wavelengths, caused by the transversal plasmonic excitation over the width at 510 nm and the more pronounced longitudinal excitation along the length of the particles at 763 nm. The width of the particles averaged 8.1 nm (+0.90/−1.0 nm), the length measured 29 nm (+7.2/−6.3 nm). Regarding the bimetallic nanoparticles, the gold–palladium rods also showed two absorption peaks at around 518 nm (transversal) and 1080 nm (longitudinal, see Figure 1E). Their shape can be described as homogeneously square cuboid and their dimensions were measured to average 103 nm (+14/−25 nm, length) and 19 nm (+3.8/−4.8 nm, width). The gold–platinum rods (Figure 1F) were also homogeneous in structure with round tips and exhibited maximum absorption wavelengths at 515 nm (transversal) and 1100 nm (longitudinal). Their length was an average 110 nm (+25/−19 nm) and their width 19 nm (+3.3/−5.0 nm). In Figure S1 (Supplementary Materials) the original spectra of the AuPd and AuPt nanorods are displayed, showing both absorption peaks.

To characterize the surface charge and stability of the nanoparticle solutions, the zeta potential was determined. The gold nanospheres exhibited an average zeta potential of $\zeta = -45$ mV. A negative zeta potential is typical for citrate-stabilized gold nanoparticles [83–85]. The gold nanocubes, on the other hand, showed a positive zeta

potential of ζ = +49 mV. The positive charge of the gold nanocubes was caused by the coating with CTA^+ [86]. Likewise, the zeta potential of the nanorods (CTAB) and nanoprisms (CTAC) was ζ = +61 and ζ = +64 mV respectively. The bimetallic nanorods in CTAC exhibited a positive zeta potential of average ζ = +58 (AuPd-nanorods) and ζ = +47 mV (AuPt-nanorods). Regarding the risk of agglomeration, the solutions were assumed to be stable, since the measured values of all nanoparticle solutions were above or below the stability limit of +/ −30 mV [87].

2.2. Catalytic Methylene Blue Reduction with Au-, AuPd- and AuPt-Nanoparticles

The reduction of methylene blue using sodium borohydride in the presence of the metal nanoparticles as catalysts was selected as a model reaction to study the catalytic activity of the nanoparticles. In this process, the metal nanoparticles serve as an additional electron supplier or mediator. For this purpose, the methylene blue and BH_4^- ions are adsorbed on the surface of the gold particles, whereby the (activated) particle transfers electrons to the adsorbed methylene blue molecules for reduction. These are consequently reduced to leucomethylene blue (see Figure 2) [80]. The reaction progress over time can be followed by UV/Vis spectroscopy.

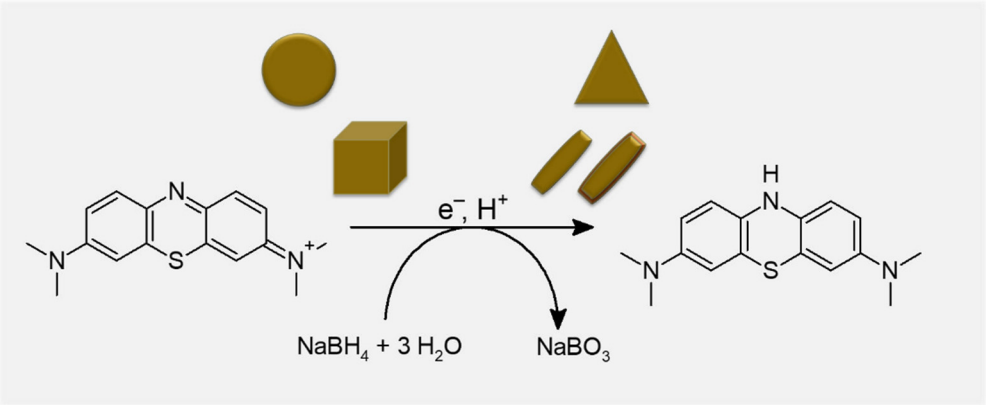

Figure 2. Reaction scheme of the conversion of methylene blue to leucomethylene blue by sodium borohydride in the presence of different gold bimetallic nanoparticles as catalysts.

2.2.1. Methylene Blue Reduction with Reference Solutions (without AuNPs)

Methylene blue showed a strong absorption peak at a wavelength of 665 nm which arises from the n-π*-transition within the molecule [82]. Before examining the individual gold nanoparticles, a reference measurement was carried out in duplicate with water without the addition of nanoparticles (Figure 3). As can be seen from the decreasing absorbance of the methylene blue peak at λ = 665 nm, a degradation of up to 18.6% or 19.9% took place within the set reaction time of 30 min. This conversion occurred solely from the reducing effect of sodium borohydride.

Furthermore, reference measurements were carried out with the supernatants of the shape-anisotropic gold nanoparticle solutions, since the ligands CTAC and CTAB used to stabilize the nanoparticles can also show a reductive effect. In the literature, it was observed that the 4-nitrophenol absorption peak was constantly decreasing upon CTAB addition of 10 mM concentration [80]. With the exception of gold nanospheres, all gold nanoparticle solutions used in our own experiments contained CTAB or CTAC as a surfactant, which is why the degradation effect of these compounds was verified (see Figure S2A–E, Supplementary Materials).

The exact CTAB or CTAC concentration per particle solution cannot be accurately determined. Within the synthesis, a precise concentration of the surfactants was set, but the particles were processed several times after synthesis (washing, centrifugation, redispersion and adjustment to a standard *OD* = 1). For this reason, the supernatants were used as a reference to approximate the actual concentration. This resulted in a

methylene blue turnover of 16.8% and 34.1% (supernatant gold cubes, CTAC), 14.8% and 22.6% (supernatant gold rods, CTAB) and 43.4% and 41.7% for the supernatant of gold prisms with CTAC after the set reaction time of 30 min. The supernatants of the bimetallic nanorods showed a reaction progress of 22.1% and 24.2% (AuPd) and 39.1% and 38.7% (AuPt), both also with CTAC as surfactant.

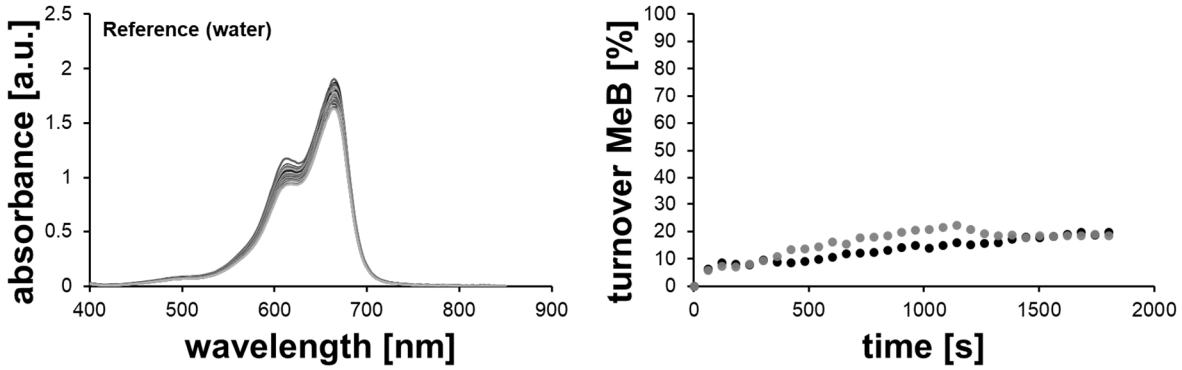

Figure 3. Absorption spectra of methylene blue from reference measurements with water over time (**left**), resulting in a turnover-time curve (**right**).

To investigate the reaction kinetics, the rate constant k of methylene blue reduction was determined from the measurements. In general, a reaction mechanism of pseudo-first order with respect to methylene blue was assumed for the reaction, since the concentration of sodium borohydride and thus of BH_4^- ions essential for reduction clearly predominated with final starting concentrations 0.034 mM for methylene blue and 4.45 mM for sodium borohydride in the reaction batch in the cuvette. Analogous to the literature, the steepest increase at the beginning of the reaction, where fastest methylene blue reduction is supposed to occur, was utilized [80]. Using the pseudo-first order time law, the rate constant k could be obtained, as shown in Equation (1).

$$[Abs_t] = [Abs_0] \cdot e^{-k \cdot t} \quad (1)$$

The measurement series with water as reference resulted in a mean rate constant of 1.38×10^{-4} s^{-1} (see measurement curves for evaluation in Figure S3, Supplementary Materials). For the reference measurements with the supernatants of the particle solutions, mean rate constants of 1.55×10^{-4} s^{-1}, 1.03×10^{-4} s^{-1} and 3.10×10^{-4} s^{-1} (supernatants Au nanocubes, rods and prisms) and 1.37×10^{-4} s^{-1} and 1.64×10^{-4} s^{-1} (supernatants AuPd and AuPt nanorods) were calculated (Figure S2, Supplementary Materials).

2.2.2. Methylene Blue Reduction with Au-, AuPd- and AuPt-Nanoparticles as Catalysts

The results of the catalytic methylene blue reduction in double determination with the different nanoparticles are shown in Figure 4A–F and Figure S4A–F Supplementary Materials.

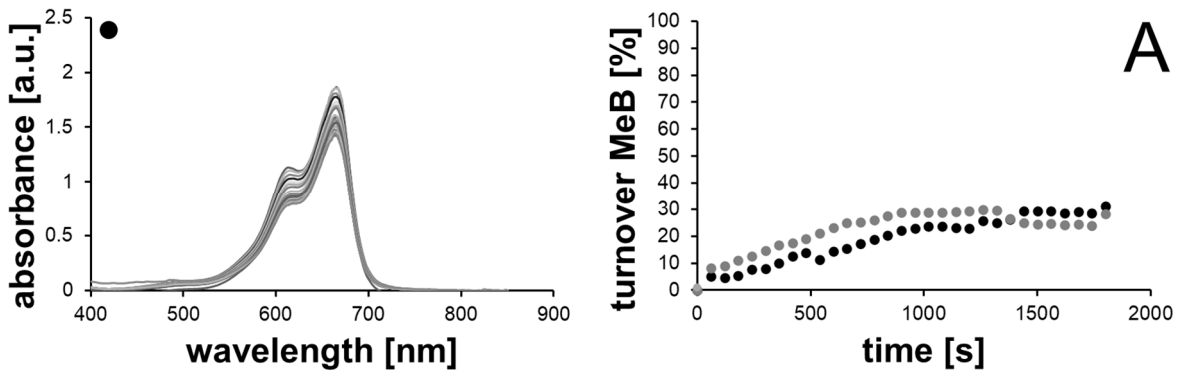

Figure 4. *Cont.*

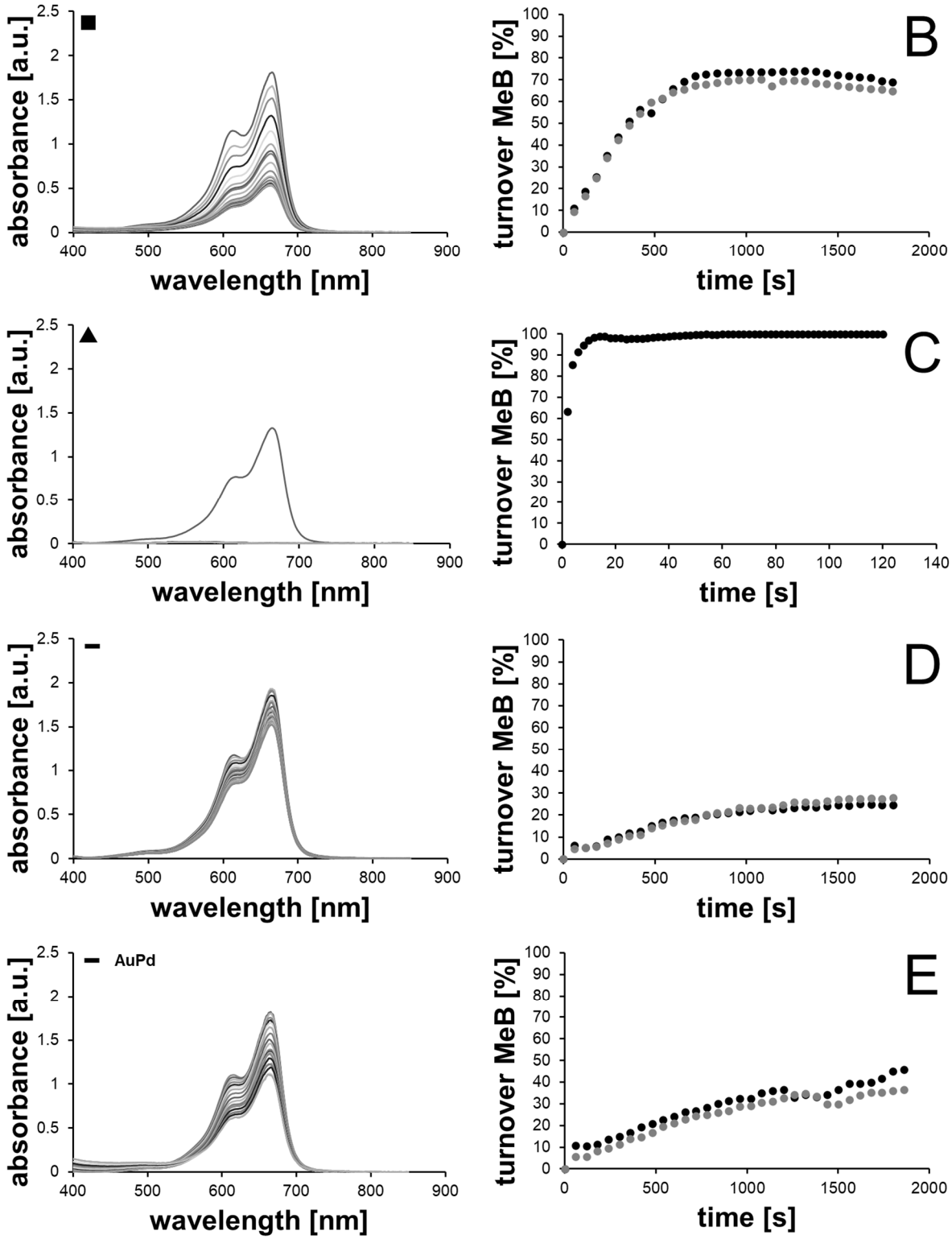

Figure 4. *Cont.*

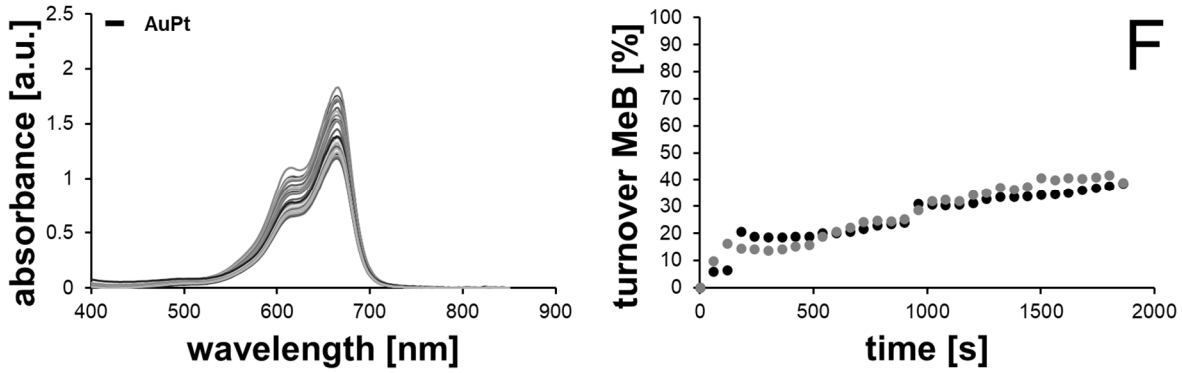

Figure 4. Absorption spectra of methylene blue from measurements with gold nanospheres (**A**), -cubes (**B**), -prisms (**C**) and -rods (**D**) as well as gold–palladium (**E**) and gold–platinum bimetallic rods (**F**), (**left**, from top to bottom) and resulting in respective turnover-time curves (**right**).

When using gold nanospheres as a catalyst (Figure 4A), a significantly higher conversion was recorded with 29.4% and 33.0%, respectively, than within the reference measurements with water (18.6% and 19.9%). Thus, there was a considerable effect due to the addition of the nanoparticles as a catalyst. The average rate constant of these series of measurements was also significantly higher than in the reference measurements and amounted to 3.40×10^{-4} s^{-1}.

In case of gold nanocubes (Figure 4B), an even stronger conversion of methylene blue to leucomethylene blue was measured within the 30 min reaction time. The turnover was 69.0% and 64.7%, respectively, and the averaged rate constant of the reaction was 1.80×10^{-3} s^{-1}, which is significantly faster compared to the experiments with gold nanospheres. Likewise, a clear effect of the nanoparticles was evident, since the reference measurements with the supernatant of the gold nanocubes solution yielded conversions of only 16.8% and 34.1%, respectively, and a rate constant of $k = 1.55 \times 10^{-4}$ s^{-1}.

With gold nanoprisms, a complete conversion of methylene blue could be achieved from the chosen set of parameters (see Figure 4C). Due to the complete conversion of methylene blue after 2 min reaction time, further measurements were carried out, in which the absorbance was logged every 2 s. A conversion of 100% was determined after 62 s reaction time. The rate constant was 0.35 s^{-1}, even though it was no longer reasonable to consider a pseudo-first order reaction, since a constant, almost linear degradation of the methylene blue took place (see evaluation curves in Figure S4C in the Supplementary Materials). Furthermore, it could be demonstrated, that once a complete reduction to leucomethylene blue (turnover of 100%) with gold prisms as catalysts was achieved, no reoxidation to methylene blue occurred as no further absorption at λ = 665 nm was measured (Figure S4C bottom).

Although the reference sample from the supernatant of the nanoprisms yielded 43.4% and 41.7% turnover after 30 min reaction time, respectively, the reaction rate was also significantly slower in this case ($k = 3.10 \times 10^{-4}$ s^{-1}).

Gold nanorods showed degradation of only 24.5% and 27.9%, respectively (see Figure 4D). The average rate constant obtained was 2.83×10^{-4} s^{-1}. The degradation values of the reference sample were lower with 14.8% and 22.6%, respectively, and the degradation was much slower with a rate constant of $k = 1.03 \times 10^{-4}$ s^{-1}.

Regarding the bimetallic nanorods, an average turnover of 41.2% could be achieved in case of AuPd nanorods and 38.9% for AuPt nanorods as catalysts (Figure 4E,F, respectively). Compared to the reference solutions, a higher turnover resulted in these cases as well, since the supernatants only yielded an average 23.2% (AuPd rods) and 30.1% (AuPt rods). In comparison to pure gold nanorods, the utilization of bimetallic nanorods resulted in a higher methylene blue to leucomethylene blue turnover in both cases, which was also occurring faster when regarding the rate constant k. For AuPd nanorods, k could be calculated to 3.69×10^{-4} s^{-1} and to 3.10×10^{-4} s^{-1} in case of AuPt nanorods utilizing

the pseudo-first order time law (Figure S4). These reaction rate constants were higher than for pure gold nanorods at 2.83 × 10^{-4} s^{-1} and significantly higher compared to the respective reference solutions with the AuPd supernatant at 1.37 × 10^{-4} s^{-1} and the AuPt supernatant at 1.64 × 10^{-4} s^{-1} (see Figure S2). These results demonstrate well that the addition of a typically catalytically active second metal like palladium or platinum is beneficial in order to achieve a more effective dye reduction, whereby AuPd delivered a higher average turnover but with a lower reaction rate constant than AuPt nanorods. These slightly different effects might be ascribed to the different morphology of the second metal on the gold nanorod structure of the different nanorods, with AuPd rods exhibiting a cuboid and therefore more edgy structure than the roundish AuPt nanorods. The AuPt rods also exhibited a patchier structure with spots of the second metal all over the surface, compared to the AuPd nanorods with a closed palladium shell. Most notably, differences arising from the different materials in the reaction behavior were possible.

Overall, although a degradation effect of the CTAB or CTAC was observed, the influence of the nanoparticles was clearly evident in each series of experiments, as the turnover of methylene blue after 30 min reaction time and the rate constants of the reactions turned out to be much higher.

The fluctuations in the measured absorbances and thus in the methylene blue conversion values (e.g., in case of nanospheres and bimetallic nanorods) can be explained either by interference of the UV/Vis radiation with hydrogen bubbles formed from the conversion of the sodium borohydride or by reoxidation of the methylene blue by atmospheric oxygen in the measurement cuvette. The plasmonic effect initiated by the Xenon flash lamp as light source in the utilized spectrophotometer [88] may not be disregarded, since the nanoparticles all showed resonance in the applied range of light (compare Figure 1). In this way, besides the generated electrons supporting the methylene blue reduction, at the same time generated holes can lead to reoxidation of leucomethylene blue. Furthermore, the sometimes steep increase of turnover between the points at reaction time 0 s and 60 s can be ascribed to the process of chemical addition to the methylene blue solution (preparation of fresh $NaBH_4$ solution, addition of $NaBH_4$ solution, nanoparticle solution and mixing through manual shaking) and therefore slightly different starting conditions at these points of reaction occur.

Besides the nanoparticle structure and the impact of surfactants, an important factor influencing the catalytic degradation is the available catalyst surface as gold surface. Therefore, we compared the calculated surface areas per particle sample with the achieved turnover and reaction rate constant *k* respectively (see overview in Table 1).

Table 1. Calculated catalyst surface areas and key figures of the methylene blue reduction (c_0 = 34 µM) classified by utilized particle samples and respective reference solution.

Sample	Available Catalyst Surface [10^{11} nm^2]	$k_{averaged}$ [10^{-4} s^{-1}]	Turnover after 30 min [%]	Final Concentration of MeB [µM]
reference	-	1.38	18.6/19.9	27.7/27.2
gold nanospheres	5.64	3.40	29.4/33.0	24.0/22.8
reference	-	1.55	16.8/34.1	28.3/22.4
gold nanocubes	2.82	18.0	69.0/64.7	10.5/12.0
reference	-	3.10	43.4/41.7	19.2/19.8
gold nanoprisms	17.4	3500	100/100	0
reference	-	1.03	14.8/22.6	29.0/26.3
gold nanorods	24.1	2.83	24.5/27.9	25.7/24.5
reference	-	1.37	22.1/24.2	26.5/25.8
gold-palladium nanorods	9.05	3.69	45.7/36.6	18.5/21.6
reference	-	1.64	25.1/35.0	25.5/22.1
gold-platinum nanorods	12.4	3.10	39.1/38.7	20.7/20.8

As can be seen, the bare catalyst surface area of the different particle types did not seem to impact the reduction reaction. For example, the gold nanorods with the largest theoretically calculated surface area only achieved the lowest turnover after the set reaction time of 30 min, whereas gold nanoprisms showed a total conversion and also the utilization of gold cubes as catalysts with the smallest surface area resulted in a relatively high turnover of around 65–70%. Although the free surfactant showed an influence on the reaction, the main impact on the reaction behavior is attributed to the particle shape. As already discussed, the short-term excitation during the measurement can result in hot spots with higher electron density in the particle corners and edges of the shape-anisotropic particles. Since shape-anisotropic particles in general exhibited more surface atoms essential for high catalytic activity than gold nanospheres [72]; the facets at the surface of these particles seem to enhance the dye adsorption and electron transport for the reduction process. Both effects can lead to an accelerated reaction in case of shape-anisotropic nanoparticles. Furthermore, the effect of the addition of the catalytic active metals palladium and platinum was well visible, since a higher turnover was achieved than in the case of pure gold nanorods despite a lower catalyst surface area.

A literature comparison of the obtained turnover and rate constants can only be made in case of gold nanospheres, since no analogous experiments with shape-anisotropic gold nanoparticles are available for methylene blue degradation. However, a general comparison with other studies can be carried out. In the literature mentioned in the introduction (describing the reduction of 4-nitroaniline reduction with sodium borohydride utilizing gold nanospheres, -rods and -prisms), other than in our studies with methylene blue, gold nanospheres (45 nm) showed the highest turnover with a rate constant of 1.66 s^{-1} with a catalyst surface area of 6400 nm^2, a particle number of 1.1 $\times$ 10^{20} per mL and a complete reaction time of 64 min. With all utilized particle solutions, complete turnover was achieved after 2 h reaction time. However, as our studies showed, the catalyst surface area is of subordinate impact, as also here the samples with the highest available gold area (gold nanorods) are not the ones with the fastest turnover [78]. In the *p*-nitrophenol reduction with sodium borohydride and gold nanorods and spheres, the shape-anisotropic nanoparticles (nanorods) were more catalytically active than the nanospheres with a complete turnover time of 50 s, with 0.1 mol L^{-1} $NaBH_4$ and 50 µL of a 2.0 $\times$ 10^{-4} mol L^{-1} nanorod solution at room temperature. The reaction rate constant was in case of nanorods as catalysts ten times higher than that for nanospheres (nanorods = 1.0 $\times$ 10^{-3} s^{-1} to nanospheres = 1.0 $\times$ 10^{-4} s^{-1}). As a reason for this observation, the accessible number of gold atoms at the surface was given, which was higher for gold nanorods [72]. Regarding the comparison with other studies to methylene blue degradation with gold nanospheres, it can be found that the rate constant *k* in our own experiments, 3.4 $\times$ 10^{-4} s^{-1}, was slightly lower than that in the literature (8.67 $\times$ 10^{-4} s^{-1}, turnover = 75%). However, the catalyst surface area in the literature of 2.6 $\times$ 10^{13} nm^2 was higher than in our own experiments and 20 nm gold nanospheres were used. The higher catalytic activity is attributed to the particle size. In smaller particles, the gold atoms on the surface are less ordered and in a more open structure than in larger particles, making them more accessible. The surface/volume ratio also plays a role, which is larger for smaller particles [80]. For 20 nm gold nanospheres a value of 0.3 nm^{-1} is obtained; for our own used particle solutions the results were: 0.22 nm^{-1} (gold nanospheres), 0.14 nm^{-1} (gold nanocubes), 0.54 nm^{-1} (gold nanorods), 0.23 nm^{-1} (gold–palladium nanorods), 0.22 nm^{-1} (gold–platinum nanorods) and 0.55 nm^{-1} (gold nanoprisms). Therefore, this quantity also shows no correlation with the obtained conversion values when comparing the different nanoparticle solutions.

3. Materials and Methods

3.1. Chemicals and Materials

All utilized chemicals were obtained commercially and used without further purification: hydrogen tetrachloroaurate trihydrate ($HAuCl_4 \times 3H_2O$, 99.5% Au content), hydrochloric acid (37%), L-(+)-ascorbic acid for gold nanocube, -rod and -prism synthesis

(≥99%), methylene blue powder, nitric acid (≥65%), silver nitrate for gold nanorod synthesis ($AgNO_3$, 63.5% Ag content), cetyltrimethylammonium bromide (CTAB, ≥99%, used in the synthesis of the gold-palladium and gold-platinum nanorods), sodium oleate (~90%), hydrochloric acid (2 N, used in the synthesis of the gold-palladium and gold-platinum nanorods) †, silver nitrate (99.9999%, used in the synthesis of the gold-palladium and gold-platinum nanorods)†, nitric acid (0.1 N, used in the synthesis of the gold-palladium and gold-platinum nanorods)† and trisodium citrate (≥99%), were obtained from Carl Roth GmbH & Co KG (Karlsruhe, Germany). Cetyltrimethylammonium bromide for gold nanorod synthesis (CTAB, ≥99%), sodium borohydride (≥98%), potassium tetrachloroplatinate(II) (≥99.99% trace metals basis) and sodium iodide (≥99,5%) were purchased from Sigma-Aldrich Chemie GmbH (Taufkirchen, Germany). Cetlytrimethylammonium chloride (CTAC, 98%) was obtained from Fluka Chemie GmbH (Buchs, Switzerland). Sodium bromide was purchased from Merck KGaA (Darmstadt, Germany). L-(+)-ascorbic acid (99 +%, used in the synthesis of the gold-palladium and gold-platinum nanorods)† and potassium tetrachloropalladate(II) (99.99% metals basis), were obtained from Alfa Aesar Thermo Fisher (Kandel) GmbH (Kandel, Germany). For solution preparation, solely Milli-Q water (from Merck Q-POD system, Merck KGaA, Darmstadt, Germany) was used.

3.2. Characterization Methods

UV/Vis Spectroscopy

UV/Vis spectroscopy to determine the optical properties of the particle solutions was performed on a V-670 spectrophotometer (Jasco Inc., Easton, MD, USA) and a NanoDrop One^C (Thermo Fisher Scientific, Waltham, MA, USA) in glass cuvettes (104.002B-QS, 10 mm layer density, Hellma GmbH & Co. KG, Müllheim, Germany). As a reference, Milli-Q water was utilized.

Thereby the absorbance was determined and the number of particles N per mL of the nanoparticles was calculated according to Scarabelli et al. [32] (Equation (S1), Table S1, Supplementary Materials). Assuming that all particles were homogeneous in size and shape, the total surface area of all particles in one ml of solution was calculated using Equation (S2) (Supplementary Materials).

Differential Centrifugal Sedimentation

Particle number determinations of particle dispersions in dilutions used for the catalytic reaction tests were performed using differential centrifugal sedimentation with a CPS DC20000 (CPS Instruments Inc., Prairieville, LA, USA). The measurement conditions and computational parameters used for the calculations are given in the Supplementary Materials.

Scanning Electron Microscopy

SEM measurements for the determination of particle size, shape and particle size distribution of the gold nanoparticles were performed under vacuum with a FE-SEM JSM 6300F respectively FE-SEM JSM-7900F microscope system (JEOL, Akishima, Japan).

In case of the bimetallic nanorods, SEM images were taken using a Hitachi S-4800 SEM (Hitachi High-Tech Europe GmbH, Krefeld, Germany).

The analysis of the particle sizes was performed using the program Image J (version 1.53e, Wayne Rasband and contributors, National Institutes of Health, Bethesda, MD, USA).

Zeta Potential Measurements

Zeta potential measurements of as-obtained gold nanoparticles were carried out utilizing a Zetasizer ZEN3600 instrument (Malvern Instruments Ltd., Worcestershire, UK) with folded capillary disposable cuvettes (DTS 10170). The following measurement settings were applied: material = gold (Malvern), dispersant = water at a temperature of 25 °C (viscosity of 0.8872 cP, refractive index of 1.330), equilibration time for temperature adjustment = 120 s, measurement = three measurements with no waiting time and at least 10 repetitions per measurement. The three recorded measurements were averaged.

The bimetallic samples were measured like the gold nanoparticles mentioned above. Prior to measurements, both nanoparticle solutions were diluted in Milli-Q water in the volume ratio ψ = 1:100.

3.3. Synthesis of Metal Nanoparticles

Synthesis of Gold Nanoparticles

In total, six nanoparticle solutions were synthesized: gold nanospheres, nanocubes, nanoprisms, nanorods and bimetallic nanorods. In case of syntheses in glass flasks or glass vials with stirring rods, these were first rinsed with ethanol, acetone, isopropanol and deionized water prior to cleaning with aqua regia (volume ratio $\psi_{HCl:HNO3}$ = 3:1) for at least 10 min. Afterwards, the glassware and stirring rods were rinsed with Milli-Q water and dried under nitrogen flow.

Synthesis of Gold Nanospheres

The synthesis of the gold nanospheres was carried out following the procedure described by Bastús et al. [14] under argon atmosphere in a glass flask. In the first step, gold nuclei were prepared. For this purpose, an aqueous sodium citrate solution (2.2 mM, 150 mL) was heated for 15 min under vigorous stirring. After boiling, aqueous $HAuCl_4$ solution (25 mM, 1 mL) was added and the solution was incubated for 10 min under stirring. After cooling to 90 °C, $HAuCl_4$ solution (25 mM, 1 mL) was added again and the solution was stirred for another 30 min. Then, $HAuCl_4$ solution (25 mM, 1 mL) was added a third time, and after stirring for another 30 min, 55 mL of the gold nanoparticle solution prepared was taken and analyzed.

Synthesis of Gold Nanocubes

The nanocubes were produced by the method of Wu et al. [30] in 50 mL plastic vials. For the synthesis of seed particles, 10 mL of a solution consisting of $HAuCl_4$ (2.5×10^{-4} M) and CTAC (0.1 M) was prepared. To this solution, ice-cold $NaBH_4$ solution (0.45 mL, 0.02 M) was added under vigorous mixing on the vortex mixer. After leaving the seed particles to incubate for 1 h at room temperature, the gold nanocubes were synthesized. Therefore, two vials were prepared, each containing the same solution consisting of CTAC (0.32 g), Milli-Q water (9.625 mL), $HAuCl_4$ (250 µL, 0.01 M), NaBr (10 µL, 0.01 M), and ascorbic acid (90 µL, 0.04 M). Then, 140 µL of the seed solution was added to the first vial, which was mixed for about 5 s, and 25 µL of this solution was added to the second vial, which was also treated on the vortex mixer for about 10 s. Then the solution was incubated at room temperature for 15 min and centrifuged at 8000 rpm for 10 min. The supernatant was removed, the particles redispersed in Milli-Q water and characterized.

Synthesis of Gold Nanoprisms

The synthesis of gold nanoprisms was performed according to Szustakiewicz et al. [34] in 15 mL glass vials with stir bars. All synthesis steps were carried out at room temperature. To prepare the seed particle solution (solution 1), CTAC solution (4.7 mL, 100 mM) and $HAuCl_4$ solution (0.025 mL, 50 mM) were mixed under stirring for 2–3 min. Then, fresh ice-cold $NaBH_4$ solution (0.3 mL, 10 mM) was added under vigorous stirring and the solution was incubated for 2 h under stirring until brown coloration occurred.

Solution 2 was prepared by mixing CTAC solution (10 mL, 25 mM), $HAuCl_4$ solution (0.0166 mL, 50 mM), ascorbic acid solution (0.02 mL, 100 mM) and seed solution (0.1 mL) under vigorous stirring for 3 s. After that, the solution was allowed to rest for 24 h.

Then, solution 3 consisting of Milli-Q water (0.39 mL), $HAuCl_4$ (0.13 mL, 50 mM) and NaI solution (0.04 mL, 10 mM) was prepared and mixed by brief vortex treatment. Finally, solution 4 was prepared from CTAC (10.2 mL, 50 mM), ascorbic acid (0.104 mL, 100 mM) and NaI solution (0.04 mL, 10 mM) and mixed briefly. Then solution 2 (0.60 mL) was added rapidly and stirred for 45 s, before solution 3 was added completely (0.56 mL) under vigorous stirring. Stirring continued for a few seconds and the purple-colored solution was allowed to stand overnight.

CTAC solution (6.413 mL, w_{CTAC} = 25%) and Milli-Q water (0.587 mL) was added to the purple nanoparticle solution and divided into two 15 mL plastic vials of 9 mL solution each. Subsequently, the solutions were allowed to rest for 24 h. Then, CTAC solution (3.8 mL, 1 M) and Milli-Q water (0.2 mL) were added to each vial and again left overnight. Both solutions were combined, 25 mL was taken, to which CTAC (16 mL, w_{CTAC} = 25%) was added in a 50 mL plastic vial and this solution was again allowed to stand overnight. The solution was centrifuged at 10,000 rpm until the particles precipitated at the bottom of the vial, the excess CTAC was removed and the particles were redispersed in Milli-Q water and characterized.

Synthesis of Gold Nanorods

The nanorods were synthesized following the prescription of Scarabelli et al. [32] in 15 mL plastic vials with stir bars. To synthesize the seed particle solution, CTAB solution (4.7 mL, 100 mM) was first placed in a water bath (T = 27 °C) and $HAuCl_4$ solution (0.025 mL, 50 mM) was added. The solution was stirred slowly for 5 min and fresh ice-cold $NaBH_4$ solution (0.3 mL, 10 mM) was added under rapid stirring (> 1400 rpm). After 10–20 s, the stirring speed was decreased (400 rpm). Once no further reaction of $NaBH_4$ was observed, since no fresh hydrogen bubbles evolved, the seed particle solution was used to prepare the gold nanorods.

For this purpose, CTAB solution (10 mL, 100 mM) and $HAuCl_4$ solution (0.1 mL, 50 mM) were incubated at 27 °C for 10 min in the water bath under gentle stirring. Ascorbic acid solution (0.075 mL, 100 mM) was added and the yellow-orange solution continued to stir until it decolorized. Then, $AgNO_3$ solution (0.08 mL, 5 mM) was added and the solution was stirred for another few seconds. Lastly, the seed solution (240 µL) was added under vigorous stirring and the solution was subsequently left untouched for 30 min at 27 °C. The particle solution was centrifuged at 10,000 rpm, the supernatant was removed and the particles redispersed in Milli-Q water. Then the gold rods were stored in the refrigerator for several days so that excess CTAB crystallized. The supernatant containing the nanorods was removed, redispersed in Milli-Q water and characterized.

Synthesis of Bimetallic Gold-Palladium/Gold-Platinum Nanorods

For the synthesis of the bimetallic particles, gold nanorods were synthesized following the procedure developed by the group of C.B. Murray [89]. Seed particles were prepared in a vigorously stirred 20 mL flat bottom glass vial heated to 30 °C in a water bath by mixing aqueous solutions of 2.16 mL 93 mM CTAB, 20 µL of 25 mM $HAuCl_4$ and 20 µL freshly prepared 60 mM $NaBH_4$. After two minutes, the stirring was stopped and the vial was loosely capped and kept at 30 °C. For the growth of the gold nanorods, 4.255 g CTAB and 761 mg sodium oleate were dissolved in 300 mL water in a water bath at 30 °C under slow stirring. After everything was dissolved, 4.3 mL of 10 mM silver nitrate were added and the solution was incubated for 30 min. Subsequently, 7.1 mL of 25 mM $HAuCl_4$ was added under slow stirring; the solution turned orange and was decolorized over the course of ten minutes. Once the solution turned clear, 18 mM of 2 M HCl was added and the solution was incubated for 15 min. Under now vigorous stirring, 727 µL of 100 mM ascorbic acid was added and after 30 s, 150 µL of the prepared seeds were added. After 30 s, the stirring was stopped and the reaction set was incubated for 12 h at 30 °C.

The resulting dispersion was centrifuged at 3900× g for 60 min, the supernatant discarded and the pellets pooled and redispersed in water to yield 25 mL of dispersion. For selective flocculation of the gold nanorods, 2.2 g of CTAB were added and the dispersion was incubated at 30 °C for 24 h. The resulting supernatant was discarded and the precipitate redispersed in 50 mL of water, centrifuged at 3900× g for 60 min, the supernatant discarded and the pellet redispersed in 50 mL water. The centrifugation was repeated and the pellet redispersed in 25 mL water.

For the synthesis of the gold–palladium particles, in a stirred 20 mL flat-bottom glass vial in a water bath at 95 °C, 1.495 mL of water, 2.5 mL of 100 mM CTAC and 200 µL of the purified gold nanorods were mixed. Then, 25 µL of 250 mM NaOH, 31.3 µL of

20 mM K_2PdCl_4 dissolved in 100 mM HNO_3 and 750 µL of 20 mM ascorbic acid were added in sequence and the reaction was incubated in a capped vial for 5 min.

The gold–platinum particles were synthesized like the gold–palladium particles in our previous experiments [90]; here 1.240 mL of water, 2.5 mL of 100 mM CTAC and 200 µL of the purified gold nanorods were mixed and 62.5 µL of 10 mM K_2PtCl_4 and 1000 µL of 20 mM ascorbic acid added in sequence.

3.4. Conduction of Methylene Blue Reduction

Preparation of the Particle Solutions

Each of the nanoparticle solutions prepared was adjusted to an optical density of *OD* = 1 as a standard prior to use. In case of gold nanospheres, -cubes and –prisms exhibiting only one absorption peak in the region 500–550 nm, the maximum absorption wavelength was chosen for this purpose. In case of gold nanorods and bimetallic nanorods, the transversal plasmonic absorption peak also in the region 500–550 nm was selected. For this purpose, the solution of gold nanospheres and cubes had to be diluted with Milli-Q water and the solutions of gold nanorods and gold prisms had to be concentrated. For this purpose, the gold nanoparticle solutions were each divided into four 2 mL Eppendorf vials and centrifuged at 8000 rpm until a precipitate of particles was observed at the bottom of the vials. The supernatant was removed, the samples combined, and the optical density adjusted by successive addition of Milli-Q water and analysis by UV/Vis. Gold–palladium nanorods and the gold–platinum nanorods were first adjusted to an *OD* = 1. Therefore, gold–platinum nanorods and gold–palladium nanorods were concentrated similar to the process as described for gold nanorods and prisms by centrifugation at 5000 rpm for 5 min. Both bimetallic nanorod samples were then washed twice prior to use. By centrifugation at 5000 rpm for 5 min, the supernatant was removed and the particles were redispersed in the same volume of water in order to keep the optical density unchanged. The calculated concentration of the particles was validated using differential centrifugal sedimentation (Supplementary Materials, Table S1).

Preparation of the Reference Solutions

As reference solutions for the catalytic degradation of methylene blue, water (gold nanospheres) or the supernatant of the particle solutions (gold nanocubes, -rods and -prisms and bimetallic nanorods) were used after catalytic testing of the respective nanoparticle solution. Therefore, the supernatant of the already catalytically used colloidal particle solutions with *OD* = 1 was centrifuged for 10 min at 8000 rpm (gold nanoparticles) and 5 min at 5000 rpm (bimetallic nanorods) respectively; the supernatant was then collected and catalytically tested.

Experimental Setup of the Catalytic Reaction

For the testing of the different AuNP solutions as catalysts for the methylene blue reduction, the experimental approach of Piella et al. [80] was followed, adjusting the amounts of reagents to the available cuvette size of 700 µL; for manufacture see Section 3.2. In a first step, methylene blue solution (1 mM) was prepared from methylene blue powder and ultrapure water. Then, the methylene blue solution (17 µL, 1 mM) was added to the cuvette as well as Milli-Q water (444 µL) and a stirring rod (PTFE, 2 × 2 mm, Cowie Technology Group Ltd., Middlesbrough, UK). Directly after freshly prepared $NaBH_4$ solution (22 µL, 100 mM) was added, the respective nanoparticle solution was added (1.1 µL). In the case of reference measurements, this volume was substituted by water or clear supernatant of the respective particle solution. The solution was mixed by manual shaking and shaken again briefly after addition of the $NaBH_4$ solution and UV/Vis measurements (NanoDrop One^C, Thermo Fisher Scientific, Waltham, MA, USA) were used to follow the reduction of the methylene blue every 60 s. The catalytic tests were carried out at room temperature (22 °C) in a measurement range of 190–850 nm. Thereby, the reaction batch was permanently stirred in the cuvette. In case of reduction within a few minutes, the measurements were

repeated every 2 s. For leveling out the obtained data, the absorption values at 850 nm of the respective data set were subtracted from all other values.

4. Conclusions

In our studies we showed that the addition of gold or bimetallic nanoparticles strongly catalyzes the methylene blue reduction to colorless leucomethylene blue by sodium borohydride. Furthermore, we have shown that differently shaped gold nanoparticles lead to different results. The shape-anisotropic nanoparticles catalyzed the reduction reaction more strongly than the shape-isotropic gold nanospheres with exception of gold nanorods, which exhibited lower turnover and a smaller rate constant. By adding platinum or palladium as the catalytic active metal, the reaction could be accelerated and a higher turnover was achieved, indicating the catalytic impact of the second metal. In general, the average obtained methylene blue turnover was following the order Au nanoprisms > Au nanocubes > AuPd nanorods > AuPt nanorods > Au nanospheres > Au nanorods.

Parallelly, we could show, that the catalyst surface area as total metal surface area does not primarily impact the efficiency of the reduction reaction. Additionally, the influence of the surfactants CTAC and CTAB in the shape-anisotropic particle samples obviously plays a subordinate role, since the methylene blue turnover to leucomethylene blue was overall smaller for the reference samples without nanoparticles. Hereby, either electron accumulation in the edges and tips of those that were shape-anisotropic or the higher number of surface atoms can play a role in the higher turnover and accelerated reaction in case of nanocubes and nanotriangles. In contrast, gold nanorods show lower catalytic activity. The experimental findings suggest that the larger free half spaces for edge atoms in case of flat prisms and cubes could be responsible for the high catalytic activity, whereas the smaller half spaces of the multi-facet structured nanorods have much lower activity. The medium activity of gold spheres could be due to the fact that these nanobodies are not regular spheres but polynuclear assemblies of primarily formed nanocrystals (compare results of J. Polte et al. [37]), which display a certain number of edge-located gold atoms at their surface, too. The investigations on bimetallic nanorods show that the addition of the second metal-platinum and palladium is beneficial, since a higher turnover was achieved for bimetallic than for pure gold nanorods.

Supplementary Materials: The following are available online at https://www.mdpi.com/article/10.3390/catal11121442/s1, Figure S1: Equation (S1); Equation (S2); Figure S1: original absorption spectra of AuPd and AuPt nanorods with dilution in water ψ = 1:10 (A = AuPd nanorods, B = AuPt nanorods); Figure S2: Development of absorbance (left) and MeB turnover (middle) and logarithmic plot of quotient of final and starting concentration over time (right) for the MeB reduction with different particle solution supernatants as reference (A = supernatant Au cubes, B = Au prisms, C = Au rods, D = AuPd rods, E = AuPt rods); Figure S3: Development of absorbance (left) and logarithmic plot of quotient of final and starting absorbance over time (right) for the MeB reduction with water as reference; Figure S4: Development of absorbance at λ = 665 nm (left) and logarithmic plot of the quotient of concentration at t and initial absorbance over time (right) for the MeB reduction with different particle solutions as catalysts (from top to bottom, A = gold nanospheres, B = -cubes, C = -prisms, D = -rods, E = AuPd nanorods and F = AuPt nanorods); Table S1: optical density of particle solutions at λ = 400 nm, number of particles per mL and available surface area per mL.

Author Contributions: Conceptualization, H.L.K.S.S., J.J.K., A.C., J.M.K. and W.F.; methodology, H.L.K.S.S. and J.J.K.; validation, H.L.K.S.S., J.J.K., A.C., J.M.K. and W.F.; formal analysis, H.L.K.S.S. and J.J.K.; investigation, H.L.K.S.S. and J.J.K.; resources, A.C., J.M.K. and W.F.; writing—original draft preparation, H.L.K.S.S.; writing—review and editing, H.L.K.S.S., J.J.K., A.C., J.M.K. and W.F.; visualization, H.L.K.S.S., J.J.K., A.C., J.M.K. and W.F.; supervision, A.C., J.M.K. and W.F.; project administration, A.C., J.M.K. and W.F.; funding acquisition, A.C., J.M.K. and W.F. All authors have read and agreed to the published version of the manuscript.

Funding: This research was funded by the DFG project "Customized shape anisotropic bimetallic nanoparticles" (FR 1348/31-1 and KO 1403/45-1).

Institutional Review Board Statement: Not applicable.

Informed Consent Statement: Not applicable.

Data Availability Statement: Raw data utilized within this article were generated at Leibniz-Institute of Photonic Technology, Jena, Germany and at Technical University Ilmenau, Ilmenau, Germany. The data presented in this study are available on request from Wolfgang Fritzsche or regarding the synthesis and characterization of bimetallic nanorods from J. Michael Köhler (J.M.K.).

Acknowledgments: Authors would like to thank the DFG for funding of the project. Furthermore, we would like to cordially thank Franka Jahn for SEM measurements and Ekaterina Podlesnaia and Viktor Weißenborn (all Leibniz-IPHT, Jena, Germany) for assistance in the synthesis of the gold nanoparticles. We express our special thanks to the Open Access Fund of the Leibniz Association for the funding of the publication of this article.

Conflicts of Interest: The authors declare no conflict of interest.

References

1. Sarina, S.; Waclawik, E.R.; Zhu, H. Photocatalysis on supported gold and silver nanoparticles under ultraviolet and visible light irradiation. *Green Chem.* **2013**, *15*, 1814–1833. [CrossRef]
2. Linic, S.; Aslam, U.; Boerigter, C.; Morabito, M. Photochemical transformations on plasmonic metal nanoparticles. *Nat. Mater.* **2015**, *14*, 567–576. [CrossRef] [PubMed]
3. Mayer, K.M.; Hafner, J.H. Localized Surface Plasmon Resonance Sensors. *Chem. Rev.* **2011**, *111*, 3828–3857. [CrossRef]
4. Khlebtsov, N.G.; Dykman, L.A. Optical properties and biomedical applications of plasmonic nanoparticles. *J. Quant. Spectrosc. Radiat. Transf.* **2010**, *111*, 1–35. [CrossRef]
5. Eustis, S.; El-Sayed, M.A. Why gold nanoparticles are more precious than pretty gold: Noble metal surface plasmon resonance and its enhancement of the radiative and nonradiative properties of nanocrystals of different shapes. *Chem. Soc. Rev.* **2006**, *35*, 209–217. [CrossRef] [PubMed]
6. Fasciani, C.; Alejo, C.J.B.; Grenier, M.; Netto-Ferreira, J.C.; Scaiano, J.C. High-Temperature Organic Reactions at Room Temperature Using Plasmon Excitation: Decomposition of Dicumyl Peroxide. *Org. Lett.* **2011**, *13*, 204–207. [CrossRef] [PubMed]
7. Bukasov, R.; Ali, T.A.; Nordlander, P.; Shumaker-Parry, J.S. Probing the Plasmonic Near-Field of Gold Nanocrescent Antennas. *ACS Nano* **2010**, *4*, 6639–6650. [CrossRef] [PubMed]
8. Bernardi, M.; Mustafa, J.; Neaton, J.B.; Louie, S.G. Theory and computation of hot carriers generated by surface plasmon polaritons in noble metals. *Nat. Commun.* **2015**, *6*, 7044. [CrossRef]
9. Mukherjee, S.; Libisch, F.; Large, N.; Neumann, O.; Brown, L.V.; Cheng, J.; Lassiter, J.B.; Carter, E.A.; Nordlander, P.; Halas, N.J. Hot Electrons Do the Impossible: Plasmon-Induced Dissociation of H2 on Au. *Nano Lett.* **2013**, *13*, 240–247. [CrossRef]
10. Hallett-Tapley, G.L.; Silvero, M.J.; González-Béjar, M.; Grenier, M.; Netto-Ferreira, J.C.; Scaiano, J.C. Plasmon-Mediated Catalytic Oxidation of sec-Phenethyl and Benzyl Alcohols. *J. Phys. Chem. C* **2011**, *115*, 10784–10790. [CrossRef]
11. González-Béjar, M.; Peters, K.; Hallett-Tapley, G.L.; Grenier, M.; Scaiano, J.C. Rapid one-pot propargylamine synthesis by plasmon mediated catalysis with gold nanoparticles on ZnO under ambient conditions. *Chem. Commun.* **2013**, *49*, 1732–1734. [CrossRef] [PubMed]
12. Brongersma, M.L.; Halas, N.J.; Nordlander, P. Plasmon-induced hot carrier science and technology. *Nat. Nanotechnol.* **2015**, *10*, 25–34. [CrossRef] [PubMed]
13. Linic, S.; Christopher, P.; Ingram, D.B. Plasmonic-metal nanostructures for efficient conversion of solar to chemical energy. *Nat. Mater.* **2011**, *10*, 911–921. [CrossRef] [PubMed]
14. Bastús, N.G.; Comenge, J.; Puntes, V. Kinetically Controlled Seeded Growth Synthesis of Citrate-Stabilized Gold Nanoparticles of up to 200 nm: Size Focusing versus Ostwald Ripening. *Langmuir* **2011**, *27*, 11098–11105. [CrossRef] [PubMed]
15. Bastus, N.G.; Merkoci, F.; Piella, J.; Puntes, V. Synthesis of Highly Monodisperse Citrate-Stabilized Silver Nanoparticles of up to 200 nm: Kinetic Control and Catalytic Properties. *Chem. Mater.* **2014**, *26*, 2836–2846. [CrossRef]
16. Brust, M.; Walker, M.; Bethell, D.; Schiffrin, D.J.; Whyman, R. Synthesis of thiol-derivatised gold nanoparticles in a two-phase Liquid–Liquid system. *J. Chem. Soc. Chem. Commun.* **1994**, *7*, 801–802. [CrossRef]
17. Turkevich, J.; Stevenson, P.C.; Hillier, J. A study of the nucleation and growth processes in the synthesis of colloidal gold. *Discuss. Faraday Soc.* **1951**, *11*, 55. [CrossRef]
18. Frens, G. Controlled Nucleation for the Regulation of the Particle Size in Monodisperse Gold Suspensions. *Nat. Phys. Sci.* **1973**, *241*, 20–22. [CrossRef]
19. Gilroy, K.D.; Ruditskiy, A.; Peng, H.-C.; Qin, D.; Xia, Y. Bimetallic Nanocrystals: Syntheses, Properties, and Applications. *Chem. Rev.* **2016**, *116*, 10414–10472. [CrossRef]
20. Henning, A.M.; Watt, J.; Miedziak, P.J.; Cheong, S.; Santonastaso, M.; Song, M.; Takeda, Y.; Kirkland, A.I.; Taylor, S.H.; Tilley, R.D. Gold–Palladium Core–Shell Nanocrystals with Size and Shape Control Optimized for Catalytic Performance. *Angew. Chem. Int. Ed.* **2013**, *52*, 1477–1480. [CrossRef]

21. Thiele, M.; Knauer, A.; Csáki, A.; Mallsch, D.; Henkel, T.; Köhler, J.M.; Fritzsche, W. High-Throughput Synthesis of Uniform Silver Seed Particles by a Continuous Microfluidic Synthesis Platform. *Chem. Eng. Technol.* **2015**, *38*, 1131–1137. [CrossRef]
22. Thiele, M.; Knauer, A.; Malsch, D.; Csáki, A.; Henkel, T.; Michael Köhler, J.; Fritzsche, W. Combination of microfluidic high-throughput production and parameter screening for efficient shaping of gold nanocubes using Dean-flow mixing. *Lab. A Chip* **2017**, *17*, 1487–1495. [CrossRef]
23. Thiele, M.; Soh, J.Z.E.; Knauer, A.; Malsch, D.; Stranik, O.; Müller, R.; Csáki, A.; Henkel, T.; Köhler, J.M.; Fritzsche, W. Gold nanocubes—Direct comparison of synthesis approaches reveals the need for a microfluidic synthesis setup for a high reproducibility. *Chem. Eng. J.* **2016**, *288*, 432–440. [CrossRef]
24. Knauer, A.; Csáki, A.; Möller, F.; Hühn, C.; Fritzsche, W.; Köhler, J.M. Microsegmented Flow-Through Synthesis of Silver Nanoprisms with Exact Tunable Optical Properties. *J. Phys. Chem. C* **2012**, *116*, 9251–9258. [CrossRef]
25. Knauer, A.; Thete, A.; Li, S.; Romanus, H.; Csáki, A.; Fritzsche, W.; Köhler, J.M. Au/Ag/Au double shell nanoparticles with narrow size distribution obtained by continuous micro segmented flow synthesis. *Chem. Eng. J.* **2011**, *166*, 1164–1169. [CrossRef]
26. De Oliveira, P.F.; Michalchuk, A.A.; Marquardt, J.; Feiler, T.; Prinz, C.; Torresi, R.M.; Camargo, P.H.C.; Emmerling, F. Investigating the role of reducing agents on mechanosynthesis of Au nanoparticles. *CrystEngComm* **2020**, *22*, 6261–6267. [CrossRef]
27. De Oliveira, P.F.; Quiroz, J.; de Oliveira, D.C.; Camargo, P.H. A mechano-colloidal approach for the controlled synthesis of metal nanoparticles. *Chem. Commun.* **2019**, *55*, 14267–14270. [CrossRef] [PubMed]
28. De Oliveira, P.F.M.; Torresi, R.M.; Emmerling, F.; Camargo, P.H.C. Challenges and opportunities in the bottom-up mechanochemical synthesis of noble metal nanoparticles. *J. Mater. Chem. A* **2020**, *8*, 16114–16141. [CrossRef]
29. De Bellis, J.; Felderhoff, M.; Schüth, F. Mechanochemical Synthesis of Supported Bimetallic Catalysts. *Chem. Mater.* **2021**, *33*, 2037–2045. [CrossRef]
30. Wu, H.-L.; Kuo, C.-H.; Huang, M.H. Seed-Mediated Synthesis of Gold Nanocrystals with Systematic Shape Evolution from Cubic to Trisoctahedral and Rhombic Dodecahedral Structures. *Langmuir* **2010**, *26*, 12307–12313. [CrossRef]
31. Pérez-Juste, J.; Pastoriza-Santos, I.; Liz-Marzán, L.M.; Mulvaney, P. Gold nanorods: Synthesis, characterization and applications. *Coord. Chem. Rev.* **2005**, *249*, 1870–1901. [CrossRef]
32. Scarabelli, L.; Sánchez-Iglesias, A.; Pérez-Juste, J.; Liz-Marzán, L.M. A "Tips and Tricks" Practical Guide to the Synthesis of Gold Nanorods. *J. Phys. Chem. Lett.* **2015**, *6*, 4270–4279. [CrossRef] [PubMed]
33. Scarabelli, L.; Coronado-Puchau, M.; Giner-Casares, J.J.; Langer, J.; Liz-Marzán, L.M. Monodisperse Gold Nanotriangles: Size Control, Large-Scale Self-Assembly, and Performance in Surface-Enhanced Raman Scattering. *ACS Nano* **2014**, *8*, 5833–5842. [CrossRef] [PubMed]
34. Szustakiewicz, P.; González-Rubio, G.; Scarabelli, L.; Lewandowski, W. Robust Synthesis of Gold Nanotriangles and their Self-Assembly into Vertical Arrays. *ChemistryOpen* **2019**, *8*, 705–711. [CrossRef] [PubMed]
35. Kumar, P.S.; Pastoriza-Santos, I.; Rodríguez-González, B.; Abajo, F.J.G.d.; Liz-Marzán, L.M. High-yield synthesis and optical response of gold nanostars. *Nanotechnology* **2007**, *19*, 015606. [CrossRef]
36. Daniel, M.-C.; Astruc, D. Gold Nanoparticles: Assembly, Supramolecular Chemistry, Quantum-Size-Related Properties, and Applications toward Biology, Catalysis, and Nanotechnology. *Chem. Rev.* **2004**, *104*, 293–346. [CrossRef]
37. Polte, J.; Herder, M.; Erler, R.; Rolf, S.; Fischer, A.; Würth, C.; Thünemann, A.F.; Kraehnert, R.; Emmerling, F. Mechanistic insights into seeded growth processes of gold nanoparticles. *Nanoscale* **2010**, *2*, 2463–2469. [CrossRef]
38. Murphy, C.J.; Sau, T.K.; Gole, A.M.; Orendorff, C.J.; Gao, J.; Gou, L.; Hunyadi, S.E.; Li, T. Anisotropic Metal Nanoparticles: Synthesis, Assembly, and Optical Applications. *J. Phys. Chem. B* **2005**, *109*, 13857–13870. [CrossRef]
39. Guo, Z.; Fan, X.; Liu, L.; Bian, Z.; Gu, C.; Zhang, Y.; Gu, N.; Yang, D.; Zhang, J. Achieving high-purity colloidal gold nanoprisms and their application as biosensing platforms. *J. Colloid Interface Sci.* **2010**, *348*, 29–36. [CrossRef]
40. Lohse, S.E.; Murphy, C.J. The Quest for Shape Control: A History of Gold Nanorod Synthesis. *Chem. Mater.* **2013**, *25*, 1250–1261. [CrossRef]
41. Major, K.J.; De, C.; Obare, S.O. Recent Advances in the Synthesis of Plasmonic Bimetallic Nanoparticles. *Plasmonics* **2009**, *4*, 61–78. [CrossRef]
42. Liu, X.; Wang, D.; Li, Y. Synthesis and catalytic properties of bimetallic nanomaterials with various architectures. *Nano Today* **2012**, *7*, 448–466. [CrossRef]
43. Zhu, C.; Zeng, J.; Tao, J.; Johnson, M.C.; Schmidt-Krey, I.; Blubaugh, L.; Zhu, Y.; Gu, Z.; Xia, Y. Kinetically Controlled Overgrowth of Ag or Au on Pd Nanocrystal Seeds: From Hybrid Dimers to Nonconcentric and Concentric Bimetallic Nanocrystals. *J. Am. Chem. Soc.* **2012**, *134*, 15822–15831. [CrossRef]
44. Csáki, A.; Thiele, M.; Jatschka, J.; Dathe, A.; Zopf, D.; Stranik, O.; Fritzsche, W. Plasmonic nanoparticle synthesis and bioconjugation for bioanalytical sensing. *Eng. Life Sci.* **2015**, *15*, 266–275. [CrossRef]
45. Steinbrück, A.; Stranik, O.; Csaki, A.; Fritzsche, W. Sensoric potential of gold–silver core–shell nanoparticles. *Anal. Bioanal. Chem.* **2011**, *401*, 1241–1249. [CrossRef] [PubMed]
46. Zopf, D.; Pittner, A.; Dathe, A.; Grosse, N.; Csáki, A.; Arstila, K.; Toppari, J.J.; Schott, W.; Dontsov, D.; Uhlrich, G.; et al. Plasmonic Nanosensor Array for Multiplexed DNA-based Pathogen Detection. *ACS Sens.* **2019**, *4*, 335–343. [CrossRef]
47. Pittner, A.; Wendt, S.; Zopf, D.; Dathe, A.; Grosse, N.; Csáki, A.; Fritzsche, W.; Stranik, O. Fabrication of micro-patterned substrates for plasmonic sensing by piezo-dispensing of colloidal nanoparticles. *Anal. Bioanal. Chem.* **2019**, *411*, 1537–1547. [CrossRef] [PubMed]

48. Szunerits, S.; Boukherroub, R. Sensing using localised surface plasmon resonance sensors. *Chem. Commun.* **2012**, *48*, 8999–9010. [CrossRef]
49. Caridad, J.M.; Winters, S.; McCloskey, D.; Duesberg, G.S.; Donegan, J.F.; Krstić, V. Hot-Volumes as Uniform and Reproducible SERS-Detection Enhancers in Weakly-Coupled Metallic Nanohelices. *Sci. Rep.* **2017**, *7*, 45548. [CrossRef]
50. Žukovskaja, O.; Agafilushkina, S.; Sivakov, V.; Weber, K.; Cialla-May, D.; Osminkina, L.; Popp, J. Rapid detection of the bacterial biomarker pyocyanin in artificial sputum using a SERS-active silicon nanowire matrix covered by bimetallic noble metal nanoparticles. *Talanta* **2019**, *202*, 171–177. [CrossRef]
51. Campion, A.; Kambhampati, P. Surface-enhanced Raman scattering. *Chem. Soc. Rev.* **1998**, *27*, 241–250. [CrossRef]
52. Yan, Y.; Radu, A.I.; Rao, W.; Wang, H.; Chen, G.; Weber, K.; Wang, D.; Cialla-May, D.; Popp, J.; Schaaf, P. Mesoscopically Bi-continuous Ag–Au Hybrid Nanosponges with Tunable Plasmon Resonances as Bottom-Up Substrates for Surface-Enhanced Raman Spectroscopy. *Chem. Mater.* **2016**, *28*, 7673–7682. [CrossRef]
53. Bailo, E.; Deckert, V. Tip-enhanced Raman scattering. *Chem. Soc. Rev.* **2008**, *37*, 921–930. [CrossRef] [PubMed]
54. Stöckle, R.M.; Suh, Y.D.; Deckert, V.; Zenobi, R. Nanoscale chemical analysis by tip-enhanced Raman spectroscopy. *Chem. Phys. Lett.* **2000**, *318*, 131–136. [CrossRef]
55. Krajczewski, J.; Kołątaj, K.; Kudelski, A. Plasmonic nanoparticles in chemical analysis. *RSC Adv.* **2017**, *7*, 17559–17576. [CrossRef]
56. Hirsch, L.R.; Stafford, R.J.; Bankson, J.A.; Sershen, S.R.; Rivera, B.; Price, R.E.; Hazle, J.D.; Halas, N.J.; West, J.L. Nanoshell-mediated near-infrared thermal therapy of tumors under magnetic resonance guidance. *Proc. Natl. Acad. Sci. USA* **2003**, *100*, 13549–13554. [CrossRef] [PubMed]
57. Amendoeira, A.; García, L.R.; Fernandes, A.R.; Baptista, P.V. Light Irradiation of Gold Nanoparticles Toward Advanced Cancer Therapeutics. *Adv. Ther.* **2020**, *3*, 1900153. [CrossRef]
58. Kim, M.; Lee, J.-H.; Nam, J.-M. Plasmonic Photothermal Nanoparticles for Biomedical Applications. *Adv. Sci.* **2019**, *6*, 1900471. [CrossRef]
59. Adleman, J.R.; Boyd, D.A.; Goodwin, D.G.; Psaltis, D. Heterogenous Catalysis Mediated by Plasmon Heating. *Nano Lett.* **2009**, *9*, 4417–4423. [CrossRef] [PubMed]
60. Stolle, H.L.K.S.; Garwe, F.; Müller, R.; Krech, T.; Oberleiter, B.; Rainer, T.; Fritzsche, W.; Stolle, A. Design of a scalable AuNP catalyst system for plasmon-driven photocatalysis. *RSC Adv.* **2018**, *8*, 30289–30297. [CrossRef]
61. Chen, X.; Cai, Z.; Chen, X.; Oyama, M. AuPd bimetallic nanoparticles decorated on graphene nanosheets: Their green synthesis, growth mechanism and high catalytic ability in 4-nitrophenol reduction. *J. Mater. Chem. A* **2014**, *2*, 5668–5674. [CrossRef]
62. Christopher, P.; Xin, H.; Linic, S. Visible-light-enhanced catalytic oxidation reactions on plasmonic silver nanostructures. *Nat. Chem.* **2011**, *3*, 467–472. [CrossRef]
63. Zhang, Z.; Zhang, C.; Zheng, H.; Xu, H. Plasmon-Driven Catalysis on Molecules and Nanomaterials. *Acc. Chem. Res.* **2019**, *52*, 2506–2515. [CrossRef]
64. Mukherjee, S.; Zhou, L.; Goodman, A.M.; Large, N.; Ayala-Orozco, C.; Zhang, Y.; Nordlander, P.; Halas, N.J. Hot-Electron-Induced Dissociation of H2 on Gold Nanoparticles Supported on SiO2. *J. Am. Chem. Soc.* **2014**, *136*, 64–67. [CrossRef] [PubMed]
65. Astruc, D. Introduction: Nanoparticles in Catalysis. *Chem. Rev.* **2020**, *120*, 461–463. [CrossRef]
66. Sharma, G.; Kumar, A.; Sharma, S.; Naushad, M.; Prakash Dwivedi, R.; ALOthman, Z.A.; Mola, G.T. Novel development of nanoparticles to bimetallic nanoparticles and their composites: A review. *J. King Saud. Univ. Sci.* **2019**, *31*, 257–269. [CrossRef]
67. Wang, D.; Villa, A.; Porta, F.; Prati, L.; Su, D. Bimetallic Gold/Palladium Catalysts: Correlation between Nanostructure and Synergistic Effects. *J. Phys. Chem. C* **2008**, *112*, 8617–8622. [CrossRef]
68. Liu, P.; Gu, X.; Zhang, H.; Cheng, J.; Song, J.; Su, H. Visible-light-driven catalytic activity enhancement of Pd in AuPd nanoparticles for hydrogen evolution from formic acid at room temperature. *Appl. Catal. B Environ.* **2017**, *204*, 497–504. [CrossRef]
69. Sui, M.; Kunwar, S.; Pandey, P.; Lee, J. Strongly confined localized surface plasmon resonance (LSPR) bands of Pt, AgPt, AgAuPt nanoparticles. *Sci. Rep.* **2019**, *9*, 16582. [CrossRef]
70. Li, J.; Saydanzad, E.; Thumm, U. Retrieving plasmonic near-field information: A quantum-mechanical model for streaking photoelectron spectroscopy of gold nanospheres. *Phys. Rev. A* **2016**, *94*, 051401. [CrossRef]
71. Narayanan, R.; El-Sayed, M.A. Catalysis with Transition Metal Nanoparticles in Colloidal Solution: Nanoparticle Shape Dependence and Stability. *J. Phys. Chem. B* **2005**, *109*, 12663–12676. [CrossRef] [PubMed]
72. De Oliveira, F.M.; de Araújo Nascimento, L.R.B.; Calado, C.M.S.; Meneghetti, M.R.; Da Silva, M.G.A. Aqueous-Phase Catalytic Chemical Reduction of p-Nitrophenol Employing Soluble Gold Nanoparticles with Different Shapes. *Catalysts* **2016**, *6*, 215. [CrossRef]
73. Priecel, P.; Adekunle Salami, H.; Padilla, R.H.; Zhong, Z.; Lopez-Sanchez, J.A. Anisotropic gold nanoparticles: Preparation and applications in catalysis. *Chin. J. Catal.* **2016**, *37*, 1619–1650. [CrossRef]
74. Wang, F.; Li, C.; Chen, H.; Jiang, R.; Sun, L.-D.; Li, Q.; Wang, J.; Yu, J.C.; Yan, C.-H. Plasmonic Harvesting of Light Energy for Suzuki Coupling Reactions. *J. Am. Chem. Soc.* **2013**, *135*, 5588–5601. [CrossRef]
75. Balanta, A.; Godard, C.; Claver, C. Pd nanoparticles for C–C coupling reactions. *Chem. Soc. Rev.* **2011**, *40*, 4973–4985. [CrossRef]
76. Wee, T.-L.E.; Schmidt, L.C.; Scaiano, J.C. Photooxidation of 9-Anthraldehyde Catalyzed by Gold Nanoparticles: Solution and Single Nanoparticle Studies Using Fluorescence Lifetime Imaging. *J. Phys. Chem. C* **2012**, *116*, 24373–24379. [CrossRef]
77. Zheng, Z.; Tachikawa, T.; Majima, T. Single-Particle Study of Pt-Modified Au Nanorods for Plasmon-Enhanced Hydrogen Generation in Visible to Near-Infrared Region. *J. Am. Chem. Soc.* **2014**, *136*, 6870–6873. [CrossRef]

78. Kundu, S.; Lau, S.; Liang, H. Shape-Controlled Catalysis by Cetyltrimethylammonium Bromide Terminated Gold Nanospheres, Nanorods, and Nanoprisms. *J. Phys. Chem. C* **2009**, *113*, 5150–5156. [CrossRef]
79. Rodrigues, T.S.; da Silva, A.G.M.; de Moura, A.B.L.; Freitas, I.G.; Camargo, P.H.C. Rational design of plasmonic catalysts: Matching the surface plasmon resonance with lamp emission spectra for improved performance in AgAu nanorings. *RSC Adv.* **2016**, *6*, 62286–62290. [CrossRef]
80. Piella, J.; Merkoçi, F.; Genç, A.; Arbiol, J.; Bastús, N.G.; Puntes, V. Probing the surface reactivity of nanocrystals by the catalytic degradation of organic dyes: The effect of size, surface chemistry and composition. *J. Mater. Chem. A* **2017**, *5*, 11917–11929. [CrossRef]
81. Naseem, K.; Farooqi, Z.H.; Begum, R.; Irfan, A. Removal of Congo red dye from aqueous medium by its catalytic reduction using sodium borohydride in the presence of various inorganic nano-catalysts: A review. *J. Clean. Prod.* **2018**, *187*, 296–307. [CrossRef]
82. Vidhu, V.K.; Philip, D. Catalytic degradation of organic dyes using biosynthesized silver nanoparticles. *Micron* **2014**, *56*, 54–62. [CrossRef]
83. Piella, J.; Bastús, N.G.; Puntes, V. Size-Dependent Protein–Nanoparticle Interactions in Citrate-Stabilized Gold Nanoparticles: The Emergence of the Protein Corona. *Bioconjugate Chem.* **2017**, *28*, 88–97. [CrossRef] [PubMed]
84. Ivanov, M.R.; Bednar, H.R.; Haes, A.J. Investigations of the Mechanism of Gold Nanoparticle Stability and Surface Functionalization in Capillary Electrophoresis. *ACS Nano* **2009**, *3*, 386–394. [CrossRef] [PubMed]
85. Tian, F.; Bonnier, F.; Casey, A.; Shanahan, A.E.; Byrne, H.J. Surface enhanced Raman scattering with gold nanoparticles: Effect of particle shape. *Anal. Methods* **2014**, *6*, 9116–9123. [CrossRef]
86. Slesiona, N.; Thamm, S.; Stolle, H.L.K.S.; Weißenborn, V.; Müller, P.; Csáki, A.; Fritzsche, W. DNA-Biofunctionalization of CTAC-Capped Gold Nanocubes. *Nanomaterials* **2020**, *10*, 1119. [CrossRef]
87. Kumar, A.; Dixit, C.K. 3—Methods for characterization of nanoparticles. In *Advances in Nanomedicine for the Delivery of Therapeutic Nucleic Acids*; Nimesh, S., Chandra, R., Gupta, N., Eds.; Woodhead Publishing: Sawston, UK, 2017; pp. 43–58. [CrossRef]
88. Thermo Fisher Scientific. NanoDrop One Microvolume UV-Vis Spectrophotometers. Available online: https://assets.thermofisher.com/TFS-Assets/CAD/Specification-Sheets/NanoDrop-One-Specifications.pdf (accessed on 1 October 2021).
89. Ye, X.; Gao, Y.; Chen, J.; Reifsnyder, D.C.; Zheng, C.; Murray, C.B. Seeded Growth of Monodisperse Gold Nanorods Using Bromide-Free Surfactant Mixtures. *Nano Lett.* **2013**, *13*, 2163–2171. [CrossRef] [PubMed]
90. Kluitmann, J.; Zheng, X.; Köhler, J.M. Tuning the morphology of bimetallic gold-platinum nanorods in a microflow synthesis. *Colloids Surf. A Physicochem. Eng. Asp.* **2021**, *626*, 127085. [CrossRef]